LOW LEVEL RF AND FEEDBACK

R. GAROBY
CERN PS/RF

The fundamental feedback loops applied in RF systems of synchrotrons are described and analysed using linear control systems theory. The classical control systems stabilizing the field in RF cavities are presented, as well as the typical beam control loops providing beam stability. The effects of high beam current ("beam loading") are examined and cures are analyzed.

1 Introduction

RF systems suffer from imperfections and drift due to all kinds of sources such as temperature, atmospheric pressure, mains ripple etc. Feedback loops are extensively applied to counteract such degradation. The basic architecture of an RF system for a synchrotron is given in Sec. 2.

The cavity control systems, which guarantee the short- to long-term stability of RF performance are described and analyzed in Sec. 3. The typical beam control loops stabilizing beam motion and providing reproducible beam characteristics are the subject of Sec. 4.

Modern accelerators are often designed for beam currents larger than the generator-induced current in a cavity, so that "beam loading" becomes a concern. The stability issue in such a regime deserves the special analysis given in Sec. 5 where the various cures are also treated.

2 Generalities

The minimum RF installation is a simple amplifier chain where the accelerating cavity is excited by the signal from an oscillator (Figure 1).

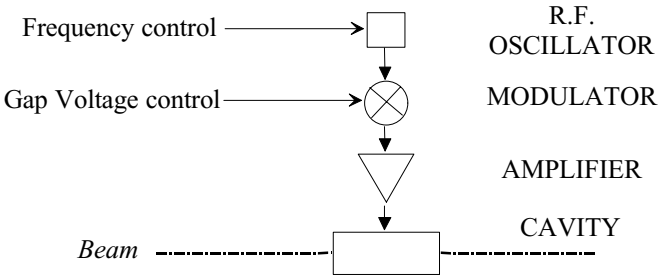

Figure 1: Minimal RF system for a synchrotron

The frequency has to be accurately controlled to centre the beam in the vacuum chamber, and the signal amplitude must be adjusted for optimum beam evolution in the longitudinal phase plane (capture at injection, matching before ejection, etc.).

With the exception of synchrotrons for leptons, where synchrotron radiation provides a natural "cooling", feedback loops are necessary to reach the accuracy and stability required for reproducible beam performance. The block diagram of such a typical RF installation is given in Figure 2. Two types of feedback loops can be distinguished:

- the hardware loops (cavity control systems analyzed in Sec. 3), which only regulate hardware performance,
- the beam control loops (Sec. 4) that use beam signals to directly stabilize beam performance.

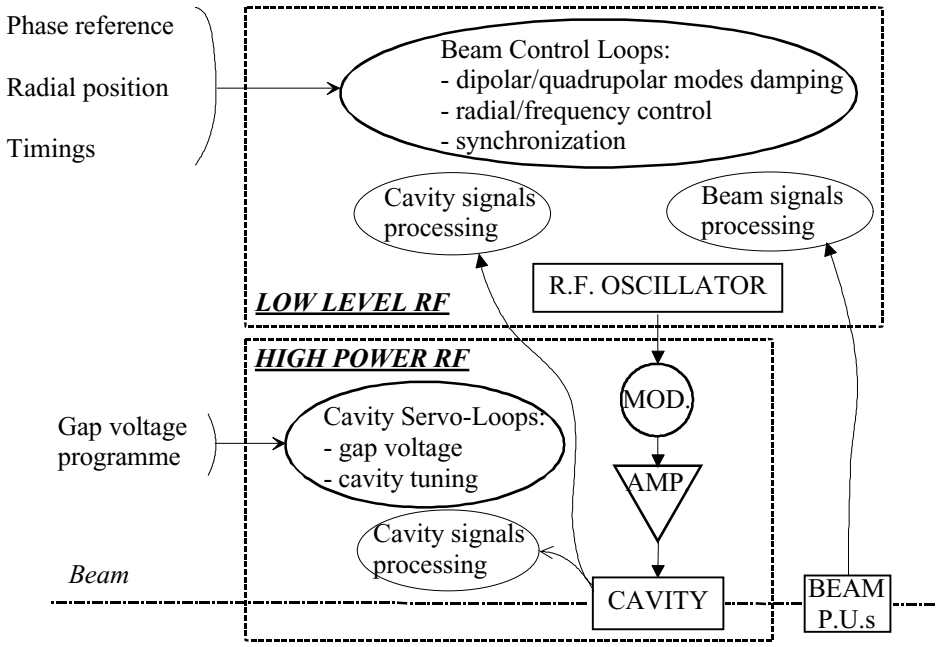

Figure 2: Typical RF system for a synchrotron

The classical tools of linear control systems theory [1] are required to analyze these systems.

3. Cavity control systems

3.1 Amplitude, phase and tuning control systems

3.1.1 Amplitude and phase modulation

The simplest control systems do not control the RF field itself but its amplitude and possibly its phase. A carrier sine-wave at ω_C rad/s modulated in amplitude by *a(t)* and in phase by *p(t)* is defined as [2]:

$$x(t) = \mathrm{Re}\left\{ \hat{X}(1 + a(t))e^{j\omega_C t + \varphi(t)} \right\} \tag{1}$$

In the limit of small modulation depth, the following approximation is valid:

$$x(t) = \mathrm{Re}\left\{ \hat{X}(1 + a(t) + j\varphi(t))e^{j\omega_C t} \right\} \tag{2}$$

System analysis requires the knowledge of the transmission of such modulations through the amplifier and the cavity resonator. Four different transfer functions are needed for a complete characterization [3]:

- $G_{aa}(j\omega)$ for the transmission of amplitude into amplitude modulation,
- $G_{pp}(j\omega)$ for the transmission of phase into phase modulation,
- $G_{ap}(j\omega)$ for the transmission of amplitude into phase modulation,
- $G_{pa}(j\omega)$ for the transmission of phase into amplitude modulation.

When the modulated carrier passes through a linear and time-invariant device with a transfer function *H(s),* the modulation transfer functions are given by [3]:

$$\begin{aligned} G_{aa}(j\omega) = G_{pp}(j\omega) = G_S(j\omega) &= \frac{1}{2}\left[\frac{H\left(j\left(\omega + \omega_C\right)\right)}{H(j\omega_C)} + \frac{H\left(j\left(\omega - \omega_C\right)\right)}{H(-j\omega_C)} \right] \\ G_{pa}(j\omega) = -G_{ap}(j\omega) = G_C(j\omega) &= \frac{j}{2}\left[\frac{H\left(j\left(\omega + \omega_C\right)\right)}{H(j\omega_C)} - \frac{H\left(j\left(\omega - \omega_C\right)\right)}{H(-j\omega_C)} \right] \end{aligned} \tag{3}$$

Example: Application to a resonator.
The impedance of a parallel RLC circuit can be written as:

$$Z(s) = \frac{2\sigma R s}{s^2 + 2\sigma s + \omega_R^2} \tag{4}$$

where ω_R is the resonant frequency (rad/s) of the circuit $\left\{\omega_R = 1/\sqrt{LC}\right\}$, σ is the damping rate (s^{-1}) $\left\{\sigma = \omega_R/(2Q)\right\}$, and Q is the quality factor $\left\{Q = R\sqrt{C/L}\right\}$.

When driven by a current generator of unity transconductance, *Z(s)* represents the system transfer function. Using Eqs. 3 and 4, the transfer functions of the phase and amplitude modulations affecting the input signal carrier (ω_C) are then:

$$\begin{aligned} G_{aa} &= G_{pp} = \frac{\sigma^2\left(1+\tan^2\varphi_Z\right)+\sigma s}{s^2+2\sigma s+\sigma^2\left(1+\tan^2\varphi_Z\right)} \\ G_{pa} &= -G_{ap} = \frac{\sigma\tan\varphi_Z s}{s^2+2\sigma s+\sigma^2\left(1+\tan^2\varphi_Z\right)} \end{aligned} \tag{5}$$

where φ_Z is defined by: $\sigma\tan\varphi_Z = \omega_R - \omega_C$ (6)

For a carrier centred at the resonance frequency ($\omega_C = \omega_R$), the system behaves like a first order low-pass filter for both types of modulation, with a 3 dB cut-off at σ rad/s, and there is no coupling between modulations:

$$\begin{aligned} G_{aa} &= G_{pp} = \frac{\sigma}{s+\sigma} \\ G_{pa} &= -G_{ap} = 0 \end{aligned} \tag{7}$$

Such a resonant circuit being a good approximation for an RF cavity, the following sections will extensively use these results, either to illustrate the effects of a detuned cavity (Sec. 3), or to justify the simplification of the system transfer function in the analysis of beam controls (Sec. 4).

3.1.2 Field amplitude control

According to Eq. 5, the same transfer functions apply for amplitude and phase modulation. Only the typical implementation of a field amplitude control system (sketched in figure 3) will then be considered in detail.

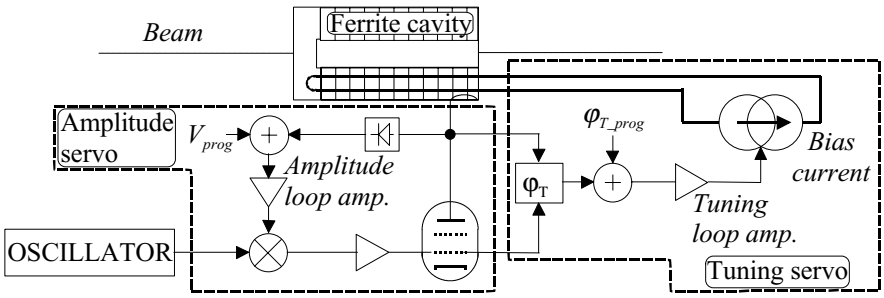

Figure 3: Typical field amplitude and tuning regulation loops

The amplitude of the signal coupled to a probe on the cavity is peak detected and compared to a V_{prog} command. The difference passes through the loop amplifier

whose output controls the amplitude of the RF signal driving the amplifier chain feeding the cavity. The functional block diagram in figure 4 describes the principle and all the transfer functions involved in the amplitude control loop.

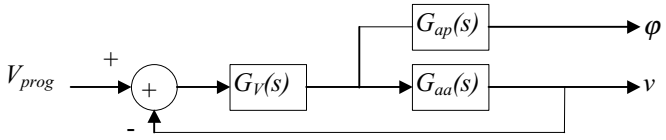

Figure 4: Block diagram of the amplitude feedback loop

The RF cavity being generally the component with the smallest bandwidth, it is justified to simplify the analysis and consider that $G_{aa}(s)$ and $G_{ap}(s)$ correspond to the cavity itself and are given by Eq. 5. $G_V(s)$ contains the characteristics of all the other components and especially of the loop amplifier and its correctors. The electrical delay will be neglected in the following analysis.

Four different cases will be systematically considered, corresponding to carrier offsets of 0 (curves labeled a), σ (curves b), 2 σ (curves c) and 3 σ (curves d) (σ being the half-3dB bandwidth of the resonator).

Open-loop transfer function without corrector. In the case where the amplifier chain is wide-band and the loop amplifier has a constant gain, the open-loop transfer function $G_{OL\_V}(s)=G_V(s)G_{aa}(s)$ is simply proportional to the cavity transfer function for amplitude modulation. When the cavity is tuned at the carrier frequency, $G_{OL\_V}(s)$ is a first order low-pass filter, according to Eq. 7, and loop stability is unconditional (curves a in figure 5). For increasing cavity detunings, $G_{OL\_V}(s)$ becomes more resonant, and stability more marginal (curves b, c and d in figure 5). A large loop gain being required at low frequencies, its effect drastically limits the possible performance of the amplitude feedback system.

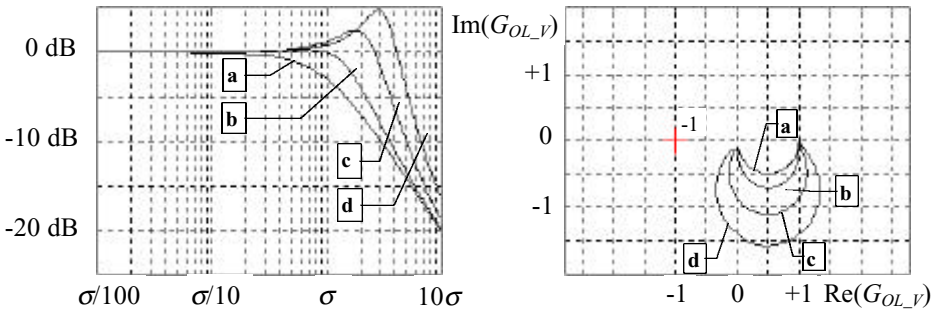

Figure 5: Open-loop Bode plot (left) and Nyquist diagram for positive frequencies (right) for an amplitude loop without corrector (G_V=1)

Open-loop transfer function with corrector. To increase the loop gain at low frequencies and preserve loop stability, a corrector is introduced with the transfer function :

$$G_V(s) = G_{V0}\left(\frac{s+\omega_{VL}}{s}\right) \tag{8}$$

The Bode plot and Nyquist diagram of $G_{OL\_V}(s)$ in figure 6 show that the system characteristics are now good enough for the closed loop performance to be investigated.

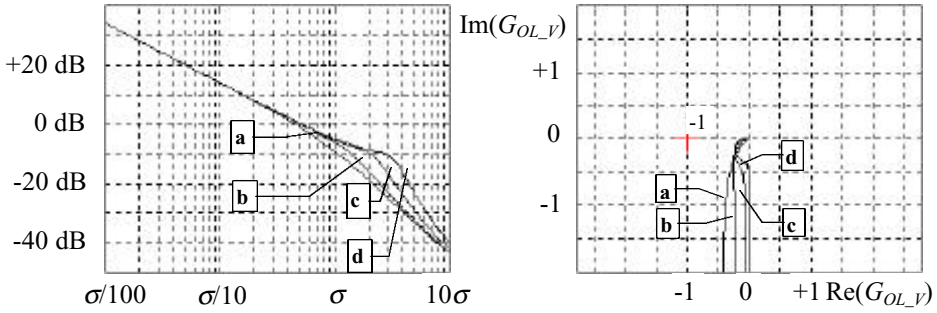

Figure 6: Open-loop Bode plot (left) and Nyquist diagram (right) for an amplitude loop with corrector (G_{V0}=0.05, ω_{VL}=10σ)

Closed-loop transfer function with corrector. Closed-loop performance of the system equipped with the corrector (Eq. 8) is illustrated by the graphs in figure 7. Amplitude control is correctly achieved, although the response is visibly distorted at the largest detunings. Phase modulation induced by the amplitude command is negligible at low modulation frequency, but becomes noticeable for a detuned cavity in the vicinity of the cut-off of the amplitude loop.

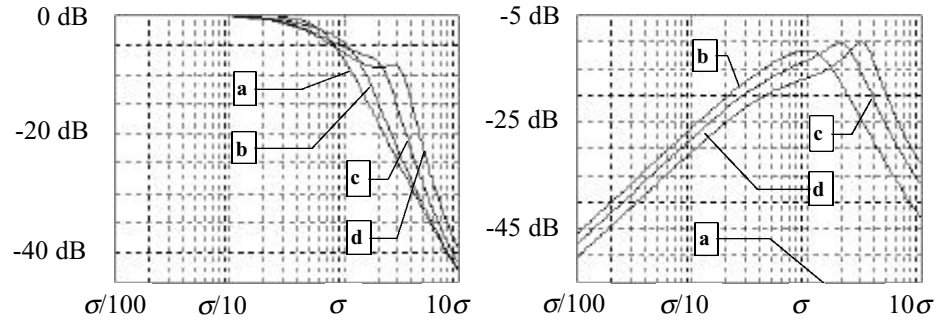

Figure 7: Closed-loop Bode plots for the amplitude feedback system (left) and for the transmission of the amplitude command into phase modulation (right)

3.1.3 Tuning control system

The typical block diagram for a tuning loop of a ferrite loaded cavity was shown in figure 3. The cavity tune is deduced from the measurement of the phase angle between cavity voltage and generator current (φ_T between cavity probe and grid 1 of the final tube). This error signal drives the current generator which biases the ferrite rings and subsequently controls the resonant frequency. The functional block diagram is given in figure 8 with the relevant transfer functions.

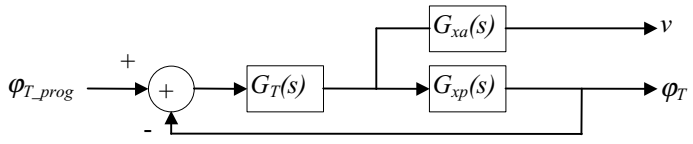

Figure 8: Block diagram of the tuning loop

The normalised tuning parameter x is defined by:

$$x = \frac{\omega_R - \omega_C}{\sigma} \tag{9}$$

For a steady excitation of the cavity by the amplifier, any change dx converts into a change in amplitude and phase of the field in the cavity. By definition G_{xa} and G_{xp} are the transfer functions for dx into amplitude and phase modulation respectively. In the case of the RLC circuit representing an RF cavity (Eq. 4) they are given by (derivation in Appendix 1):

$$\begin{aligned} G_{xa} &= \frac{-\sigma^2 \tan\varphi_Z}{s^2 + 2\sigma s + \sigma^2(1+\tan^2\varphi_Z)} \\ G_{xp} &= \frac{\sigma^2 + \sigma s}{s^2 + 2\sigma s + \sigma^2(1+\tan^2\varphi_Z)} \end{aligned} \tag{10}$$

Cavity-tuning transfer functions without corrector. G_{xa} and G_{xp} are given in figure 9 for the same carrier offsets (or detunings) as for the amplitude loop. When the cavity is tuned at the carrier frequency, G_{xp} shows a typical low-pass filter response, with a cut-off frequency at σ rad/s and G_{xa} is null. When the cavity tune is not centred on the carrier frequency, any tuning modulation converts into amplitude modulation (curves b, c and d in figure 9 right). G_{xp} then changes even at low frequencies, with a tendency to peak in gain at $|\omega_C - \omega_R|$.

For a real tuning system (figure 8), the open-loop transfer function is: $G_{OL\_T}(s) = G_T(s)G_{xp}(s)$. A corrector is inserted in the loop amplifier ($G_T(s)$) to provide a large enough open-loop gain at low frequencies and a gain smaller than one above σ, even in the presence of a certain detuning.

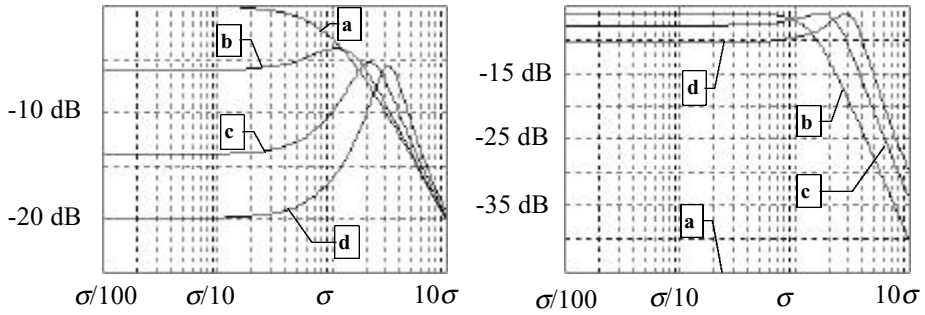

Figure 9: Bode plot of the tuning to phase (left) and tuning to amplitude (right) transfer functions without corrector (G_T=1)

Open-loop tuning transfer functions with corrector. A rudimentary corrector in $G_T(s)$ can again be of the type :

$$G_T(s) = G_{T0}\left(\frac{s+\omega_{TL}}{s}\right) \tag{11}$$

The characteristics of the corresponding Bode plot and Nyquist diagram of $G_{OL\_T}(s)$ shown in figure 10 are now satisfactory.

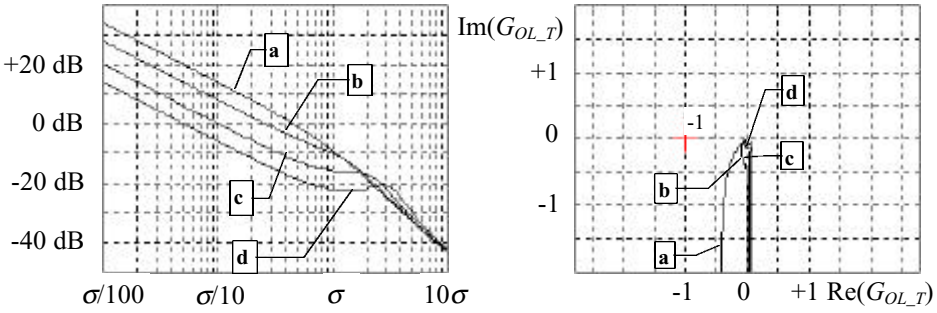

Figure 10: Open-loop Bode plot (left) and Nyquist diagram (right) for a tuning loop with corrector (G_{T0}=0.05,ω_{TL}=10σ)

Closed-loop tuning transfer function with corrector. Closed-loop performance of the tuning system equipped with the corrector (Eq. 11) demonstrates that it is unconditionally stable as illustrated by the graphs in figure 11. However, only the gain at very low frequencies is not affected by detuning. The response is low-pass, with widely varying cut-off frequency and roll-off of gain.

There is no coupling of the tuning angle command to the field amplitude when the cavity is tuned (curve a in figure 11-right), but it becomes increasingly larger when detuning goes from σ to 3 σ (curves b,c and d in figure 11-right).

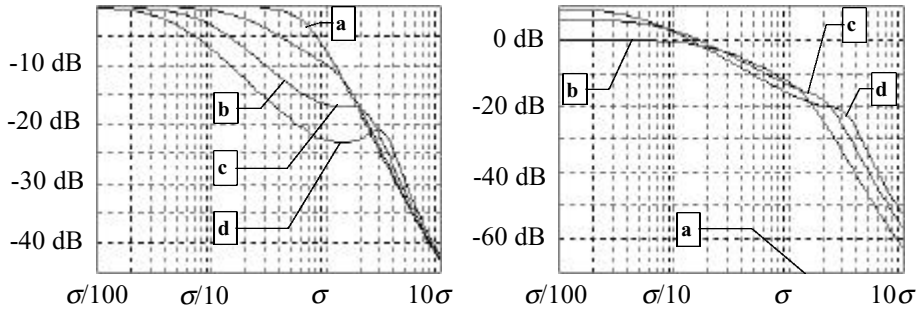

Figure 11: Closed-loop Bode plots for the tuning feedback system (left) and for the transmission of the tuning angle command into amplitude modulation (right)

3.2 Field regulation with I/Q feedback

3.2.1 I/Q modulation

A band-limited signal $x(t)$ centred on a carrier at ω_C rad/s can be expressed as the sum of two amplitude-modulated orthogonal sine-waves at the carrier frequency:

$$x(t) = x_I(t)\cos\omega_C t - x_Q(t)\sin\omega_C t \tag{12}$$

where $x_I(t)$ and $x_Q(t)$ are respectiveley the "In-phase" and "Quadrature" baseband envelopes.

Transmission through a linear time-invariant system. Contrary to amplitude/phase modulation where transmission through a linear system can only be investigated for small depth of modulation, no such limitation is needed for the analysis of I/Q transfer functions.

The transmission of $x(t)$ can be obtained from the convolution product with the impulse response $h(t)$ of the system:

$$y(t) = h(t) * x(t) \quad \Leftrightarrow \quad \mathrm{y(t)} = \int_{-\infty}^{+\infty} \mathrm{h}(\tau \qquad \tau \quad \tau \tag{13}$$

From Eqs. 12 and 13 we derive:

$$\begin{aligned} y(t) &= \left[h_{II}(t) * x_I(t) + h_{QI}(t) * x_Q(t)\right]\cos\omega_C t \\ &- \left[h_{IQ}(t) * x_I(t) + h_{QQ}(t) * x_Q(t)\right]\sin\omega_C t \end{aligned} \tag{14}$$

using the following definition of the impulse responses $h_{XY}(t)$ and their associated transfer functions:

$$\begin{aligned} & h_{II}(t) = h_{QQ}(t) = h(t)\cos\omega_C t \\ \leftrightarrow\ & H_S(j\omega) = \frac{1}{2}\left[H\left(j\left(\omega+\omega_C\right)\right) + H\left(j\left(\omega-\omega_C\right)\right)\right] \end{aligned} \tag{15}$$

$$h_{IQ}(t) = -h_{QI}(t) = -h(t)\sin\omega_C t$$
$$\leftrightarrow H_C(j\omega) = \frac{1}{2j}\left[H\left(j\left(\omega+\omega_C\right)\right) - H\left(j\left(\omega-\omega_C\right)\right)\right] \tag{16}$$

The flow-diagram in figure 12 conveniently illustrates these relations for the transmission of I/Q modulation.

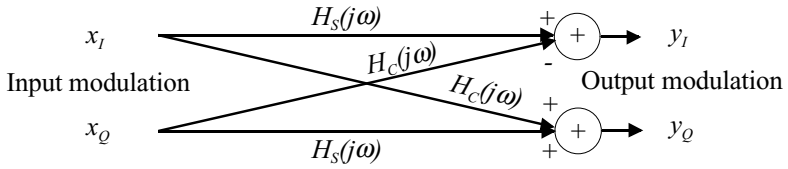

Figure 12: Transfer functions for In-phase and Quadrature signals

Example: Application to a resonator.
The impulse response of an RLC resonator (impedance given by Eq. 4) is:

$$h(t) = 2\sigma\,\mathrm{Re}^{-\sigma t}\left[\cos\omega_D t - \frac{\sigma}{\omega_D}\sin\omega_D t\right] \tag{17}$$

with:
$$\omega_D = \sqrt{\omega_R^2 - \sigma^2} \tag{18}$$

Using Eqs. 15 and 16, and with the definitions: $\Sigma\omega=\omega_D+\omega_C$ and $\Delta\omega=\omega_D-\omega_C$ we obtain:

$$h_S(t) = \sigma\,\mathrm{Re}^{-\sigma t}\left[\left(\cos\Delta\omega t + \cos\Sigma\omega t\right) - \frac{\sigma}{\omega_D}\left(\sin\Delta\omega t + \sin\Sigma\omega t\right)\right]$$
$$h_C(t) = \sigma\,\mathrm{Re}^{-\sigma t}\left[\left(\sin\Delta\omega t - \sin\Sigma\omega t\right) + \frac{\sigma}{\omega_D}\cos\left(\sin\Delta\omega t - \cos\Sigma\omega t\right)\right] \tag{19}$$

Taking the Laplace transform of these impulse responses after low-pass filtering (elimination of the terms at $\Sigma\omega$ rad/s), we finally get the transfer functions H_S and H_C characterising the resonator:

$$H_S(s) = \sigma R\left[\frac{s+\sigma\left(1-\dfrac{\Delta\omega}{\omega_D}\right)}{(s+\sigma)^2+\Delta\omega^2}\right]$$
$$H_C(s) = \frac{\sigma^2 R}{\omega_D}\left[\frac{s+\left(\sigma+\dfrac{\omega_D\Delta\omega}{\sigma}\right)}{(s+\sigma)^2+\Delta\omega^2}\right] \tag{20}$$

In the case of a carrier centred at the frequency of the damped oscillation: $\Delta\omega=\omega_D-\omega_C=0$ rad/s (notice that ω_D is given by Eq. 18 and slightly differs from ω_R), the transfer functions simplify to classical first-order low-pass filter responses:

$$H_S(s) = \frac{\sigma R}{(s+\sigma)}$$
$$H_C(s) = \frac{\sigma^2 R}{\omega_D(s+\sigma)} \tag{21}$$

3.2.2 I/Q feedback

Figure 13 shows the block diagram of an I/Q feedback control system. The vector demodulator generates the I and Q components from the cavity probe signal with respect to the reference oscillator. These are then compared to the command values I_{prog} and Q_{prog}. The differences are amplified and filtered in the Loop Corrector, whose outputs control the Vector Modulator. The cavity amplifier chain is driven by the modulator's output.

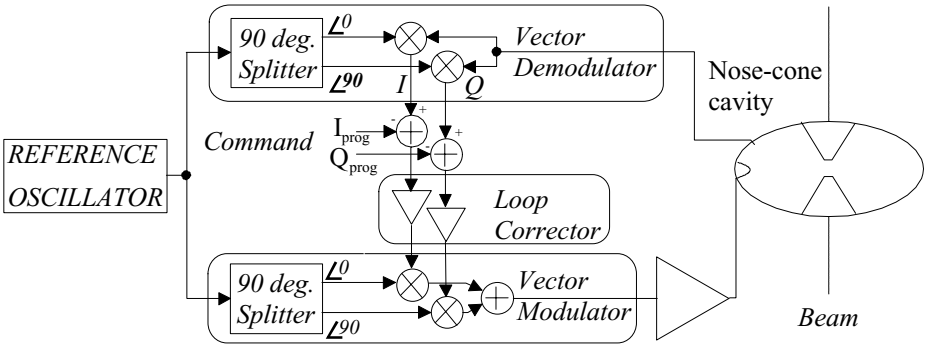

Figure 13: I/Q feedback control system

The functional block diagram in figure 14 describes the transfer functions involved in the analysis.

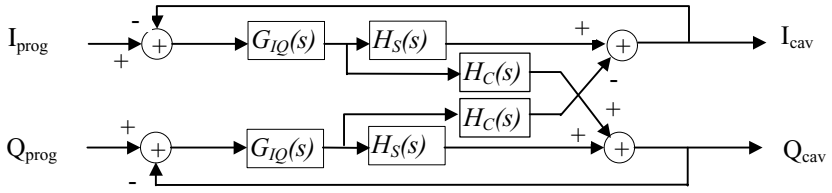

Figure 14: Block diagram of the I/Q feedback loop

H_C and H_S represent the cavity, assuming as in the previous sections that it is the element with the smallest bandwidth in the RF chain. The other elements are taken care of in G_{IQ}, and especially the loop corrector. The electrical delay is neglected.

Open-loop transfer function without corrector. By definition : $G_{OL\_IQ}=G_{IQ}H_S$. In the case where G_{IQ} is frequency independent and of unit gain, the open-loop transfer functions are given by Eq. 20, and their frequency responses are in figure 15. For a carrier centred at ω_D (curves a) the system is a first order low-pass filter, as visible in Eq. 21. When detuning increases (curves b, c and d) the gain at low frequencies decreases and peaks at the offset $\Delta\omega=\omega_D-\omega_C$. A corrector is needed to have a large enough gain in that frequency range.

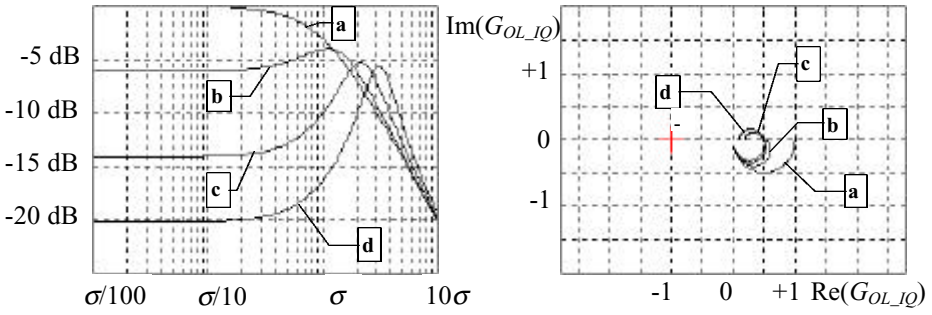

Figure 15: Open-loop Bode plot (left) and Nyquist diagram for the I (or Q) channel of an I/Q feedback loop without corrector (R =1 Ω)

Open-loop tuning transfer functions with corrector. An integrator type of corrector, similar to the ones used in the other control loops, is incorporated into G_{IQ} :

$$G_{IQ}(s) = G_{IQ0}\left(\frac{s+\omega_{IQL}}{s}\right) \qquad (22)$$

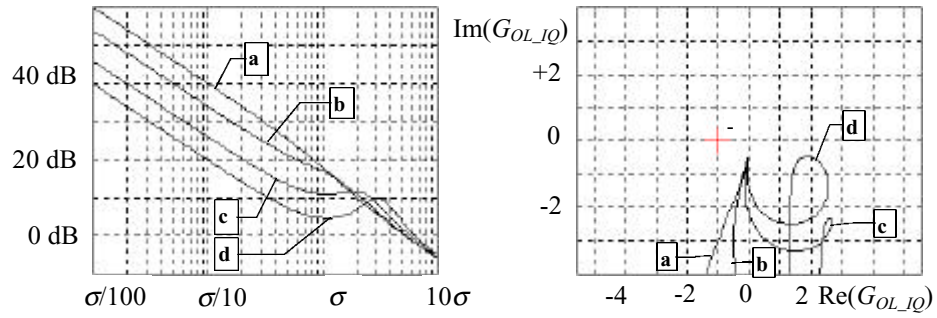

Figure 16: Open-loop Bode plot (left) and Nyquist diagram (right) for an I (or Q) loop with corrector (R=1Ω , G_{IQ0}=5, ω_{IQL}=2σ)

The corresponding Bode plot and Nyquist diagram of $G_{OL\_IQ}(s)$ are now more satisfactory, as can be seen in figure 16. The loop gain stays large in the low frequency range, while stability remains assured (figure 16 right).

Closed-loop I/Q feedback with corrector. Closed-loop performance when both the I and Q paths are closed with the corrector defined in Eq. 22 is shown in figure 17. Straight I (or Q) transmission (left graph) has a stable shape, almost unaffected by detuning, while the contrary is true for cross-coupling (right graph).

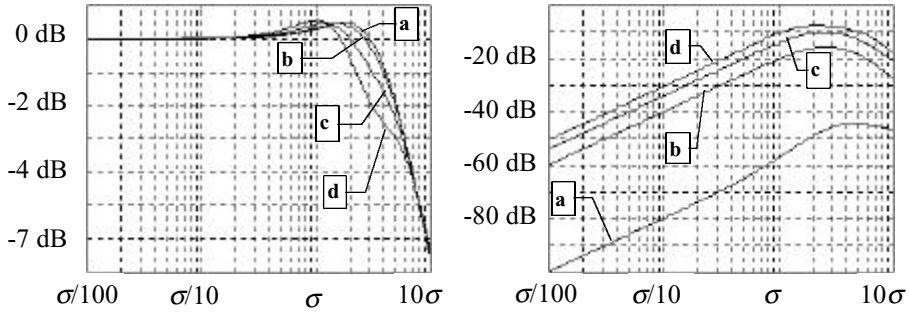

Figure 17: Closed-loop Bode plots for the I/Q feedback system: straight I (or Q) transmission (left) and cross-coupling I_{prog} to Q (right)

3.3 Comparison of amplitude/phase and I/Q control systems

The amplitude/phase (Sec. 3.1.) and I/Q (Sec. 3.2.2) feedback control systems are competing solutions for the stabilisation of the field in an RF cavity.

Table 1 : Comparison of amplitude/phase versus I/Q control systems

	Amplitude/Phase	**I/Q**
Control of field amplitude/phase	Direct (!)	Indirect (by computation)
Dynamic range in field amplitude	Limited for phase loop	Unlimited
Phase control range	< 360 deg	Unlimited
Tolerance to drift of open-loop phase-shift	Unlimited	Small (performance degradation by I/Q cross-coupling)
Operation over a large frequency range	Easy for amplitude Delicate for phase	Difficult
Implementation of DSP techniques		Prone to sophistication

Because of its simplicity, amplitude/phase control has often been favored in the past for synchrotrons, especially when phase stabilization was not mandatory and beam manipulations were rudimentary. Implementation of I/Q control puts a stringent requirement on the phase-shift across the complete loop which complicates hardware. When that condition is met, it provides a number of advantages and interesting possibilities of sophistication using modern digital signal processing techniques. A few important points of comparison are listed in Table 1.

4 Beam control loops

4.1 Beam transfer function for dipolar motion

Beam phase oscillation. By definition the stable particle is the particle that stays at the same phase φ_B (called the stable phase) with respect to the RF sine-wave in the cavity from one turn to the next. A real particle is characterised by its coordinates ($\Delta\varphi_B$, Δp) in phase and momentum with respect to that stable particle. The frequency of the RF is subject to changes $\delta\omega_{RF}$. The basic set-up considered is represented in figure 18.

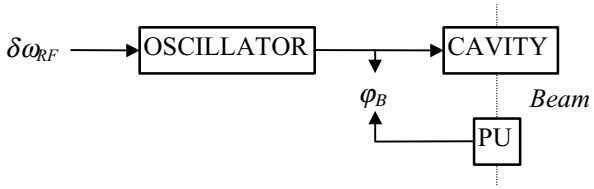

Figure 18 : Set-up for the definition of the beam transfer function for dipolar motion

The differential equations of motion for the particle in the longitudinal phase plane are then :

$$\begin{cases} \dfrac{d\Delta p}{dt} = a\cos\varphi_B \cdot \Delta\varphi_B \\ \dfrac{d\Delta\varphi_B}{dt} = b\Delta p + \delta\omega_{RF} \end{cases} \tag{23}$$

using :

$$a = \frac{qV}{2\pi R} \tag{24}$$

$$b = \left(\frac{h\beta c}{Rp}\right)\left(\frac{1}{\gamma_T^2} - \frac{1}{\gamma^2}\right) \tag{25}$$

where R is the mean radius of the synchrotron, V the peak RF voltage, h the RF harmonic number (number of RF periods per revolution), q the particle charge, p the

beam momentum, (β, γ) the standard relativistic parameters of the beam, and γ_T the γ at transition energy. Applying the Laplace transform to Eq. 23 we can derive the beam transfer function for dipolar motion :

$$B(s) = \frac{\Delta\varphi_B}{\delta\omega_{RF}} = \frac{s}{s^2 + \omega_S^2} \tag{26}$$

It represents an undamped resonator centred at the synchrotron frequency ω_S:

$$\omega_S = \sqrt{-ab\cos\varphi_B} \tag{27}$$

Beam radial position. The size of the vacuum chamber being very limited in a synchrotron, the mean radial position ΔR of the beam is an important parameter. It is measured with respect to the central orbit which corresponds to a reference rate of energy gain. This rate defines a reference phase difference $\Delta\varphi_{B\_ref}$, and any deviation of $\Delta\varphi_B$ from that value causes an energy change at the rate:

$$\frac{d\Delta E}{dt} = qf_{REV}V\cos\varphi_B \cdot (\Delta\varphi_B - \Delta\varphi_{B\_ref}) \tag{28}$$

where f_{REV} is the beam revolution frequency. Taking the Laplace transform of Eq. 28 and converting ΔE into radial position we get:

$$\frac{\Delta R}{R} = \frac{k_R}{s} \cdot (\Delta\varphi_B - \Delta\varphi_{B\_ref}) \tag{29}$$

with:

$$k_R = \omega_S^2 \frac{R}{h\beta c}\left(\frac{\gamma^2}{\gamma_T^2 - \gamma^2}\right) \tag{30}$$

4.2 Beam phase loop

A damping mechanism is needed to avoid uncontrolled beam phase oscillations and provide reproducible beam characteristics. Various methods are possible [4], all being based on feedback systems called “beam controls” which manipulate the RF according to some measured beam parameter. We will examine the typical problems associated with beam controls, considering the arrangement shown in figure 19, which is widely used in hadron synchrotrons [5, 6]. Feedback is achieved passing the beam phase information through a loop amplifier (transfer function G_{PL}) to modify the frequency of the RF oscillator.

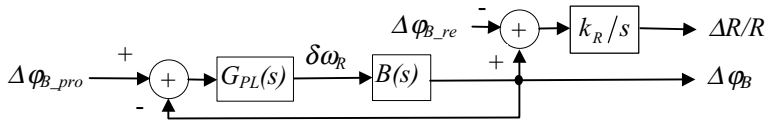

Figure 19: Block diagram of the beam phase loop

The following analysis is aimed at describing the basic principles of beam controls and important simplifications are deliberately implied which must be reconsidered for any real design:

- the complete RF amplifier chain, and consequently the cavity itself, has a unit transfer function for phase modulation. According to Eq. 5, this is only justified for tuned resonators with large bandwidth compared to the frequency range covered by the beam phase loop. This is a reasonable assumption in the case of hadron accelerators which use ferrite-loaded cavities. A first order low-pass filter with a cut-off at the half 3dB bandwidth (Eq. 7) can easily be introduced in G_{PL} if a better approximation is required.
- the electrical delay is not taken into account. This is often not justified, because the beam phase has to be fast and the phase-lag due to the delay is usually the limiting factor.

4.2.1 DC-coupled beam phase loop

Open-loop transfer function. A frequency independent gain ($G_{PL}(s) = G_{PL0}$) already provides damping of phase oscillations. Feedback stability is not a problem, as demonstrated by the plots of the open-loop gain G_{OL_PL} in figure 20 (a finite Q has been used to generate these pictures for practical illustration purpose). Aperiodic closed-loop response is obtained for $G_{PL0} > 2\omega_S$.

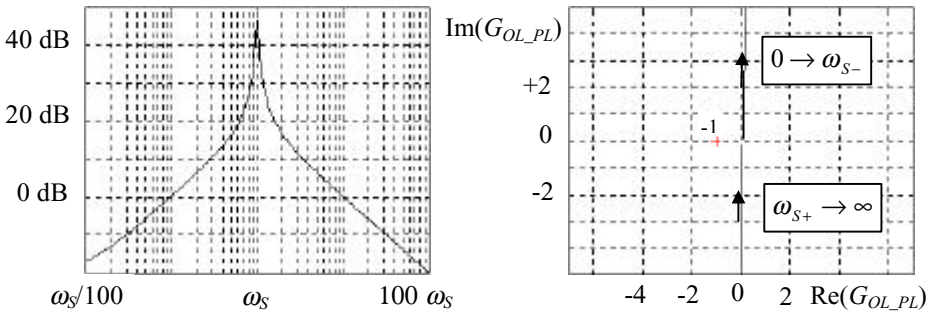

Figure 20: Open-loop Bode plot (left) and Nyquist diagram (right) for a DC coupled beam phase loop ($G_{PL0}=10\omega_S$)

Closed-loop transfer function. Operation in closed-loop gives an acceptable band-pass transfer function for the $\Delta\varphi_{B\_prog}$ command (figure 21), and the natural resonant characteristic (Eq. 26 and figure 20) disappears completely. But the transmission to the radial position has a very large gain at low frequencies down to DC, as visible in figure 21 (right where the vertical scale is arbitrary because it is machine and beam energy dependent). An adequate control of the beam radial position requires a practically unachievable accuracy on the DC value of $\Delta\varphi_{B\_prog}$.

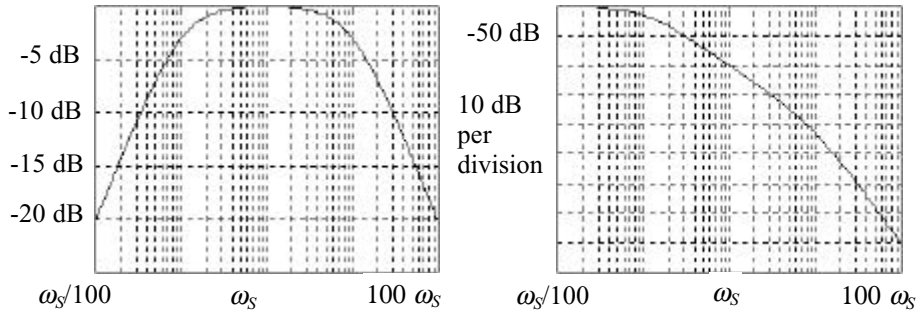

Figure 21: Closed-loop Bode plots for the DC coupled beam phase loop: transmission of the $\Delta\varphi_{B\_prog}$ command onto $\Delta\varphi_B$ (left) and onto $\Delta R/R$ (right)

4.2.2 AC-coupled beam phase loop

Using AC coupling in the phase loop (high-pass filter in the loop amplifier), the DC component of the phase error is suppressed and the DC value of $\Delta\varphi_{B\_prog}$ no longer needs to be very accurate. But then the beam radial position is defined by the programmed frequency of the RF oscillator. Fortunately modern frequency synthesis technology [3] gives highly accurate frequency control.

Open-loop transfer function. $G_{PL}(s)$ is chosen with a high-pass response given by:

$$G_{PL}(s) = G_{PL0}\left(\frac{s}{s+\omega_{PH}}\right) \tag{31}$$

where ω_{PH} must be low enough to provide acceptable gain and phase stability margins at low frequency. Typical Bode plot and Nyquist diagram of $G_{OL\_PL}(s)$ are shown in figure 22.

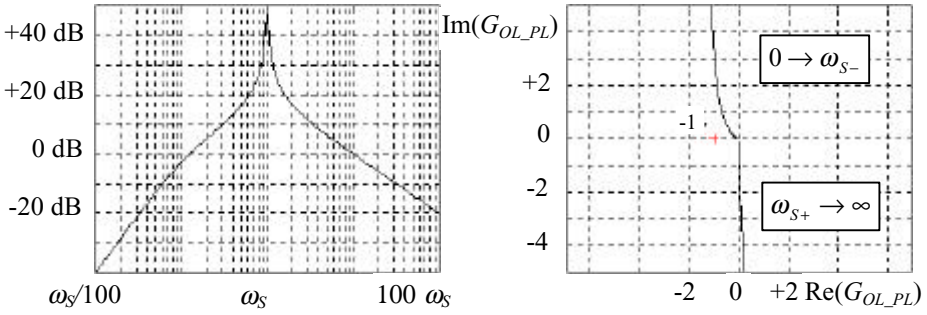

Figure 22: Open-loop Bode plot (left) and Nyquist diagram (right) for an AC coupled beam phase loop (G_{PL0}=10ω_S, ω_{PH}= ω_S/10)

Closed-loop transfer functions of an AC-coupled phase loop. The closed-loop transfer function is again of band-pass type and non-resonant (figure 23 left). The transmission to the radial position now has no gain at DC, and peaks below ω_S (figure 23 right). The accuracy of $\Delta\varphi_{B\_prog}$ at DC is no longer relevant anymore, but AC variations still need to be considered.

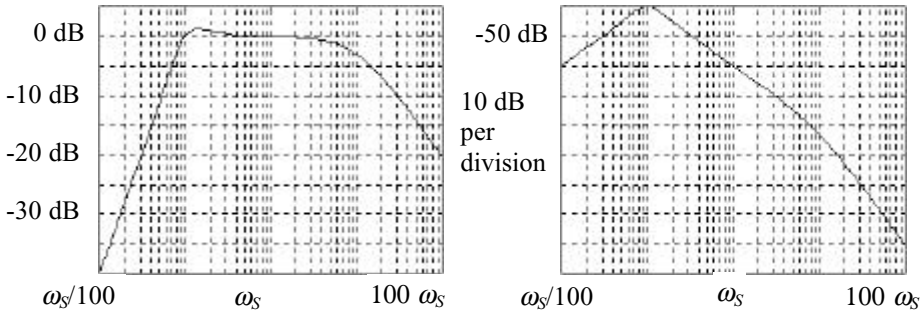

Figure 23: Closed-loop Bode plots for the AC-coupled beam phase loop: transmission of the $\Delta\varphi_{B\_prog}$ command onto $\Delta\varphi_B$ (left) and onto $\Delta R/R$ (right)

4.3 Radial loop

Sensors can be used to define the beam radial position instead of an accurate frequency control. The principle is to feed back the position error signal into the beam phase loop (figure 24) in such a way that DC and low frequency control of the radial position is achieved by the radial loop.

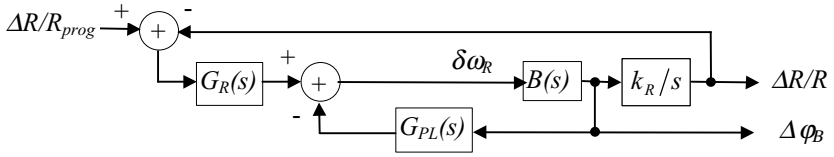

Figure 24: Block diagram of a radial loop associated with a beam phase loop

Open-loop transfer function without corrector. The first step in the investigation is to consider the case where G_R(s) is a constant ($G_R = G_{R0}$). Typical Bode and Nyquist plots are drawn in figure 25. Stability is unconditional, but the gain at low frequency is necessarily limited to cross 0 dB below ω_S. An integrator type of corrector is clearly needed.

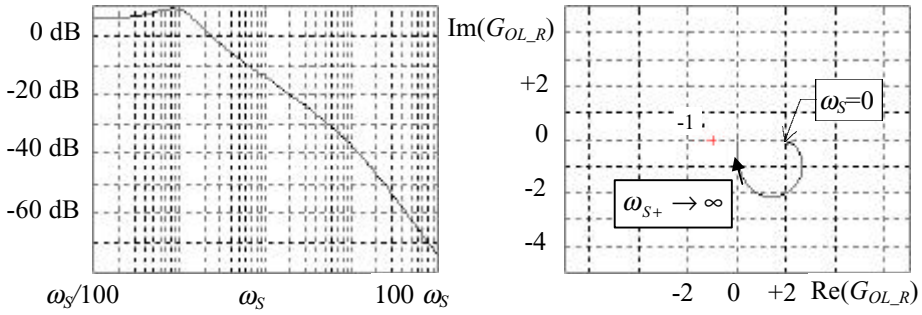

Figure 25: Open-loop Bode plot (left) and Nyquist diagram (right) for a radial loop associated to an AC-coupled beam phase loop (G_{PL0}=10ω_S, ω_{PH}= ω_S/10)

Open-loop transfer function with corrector. The following corrector is used to increase the gain at low frequency :

$$G_R(s) = G_{R0}\left(\frac{s+\omega_{RL}}{s}\right) \tag{32}$$

The resulting graphs are shown in figure 26. ω_{RL} has to be smaller than ω_S to introduce little phase lag where G_{OL_R} approaches 0 dB (here ω_{RL}=ω_S/10). Stability is then guaranteed and closed-loop operation is possible.

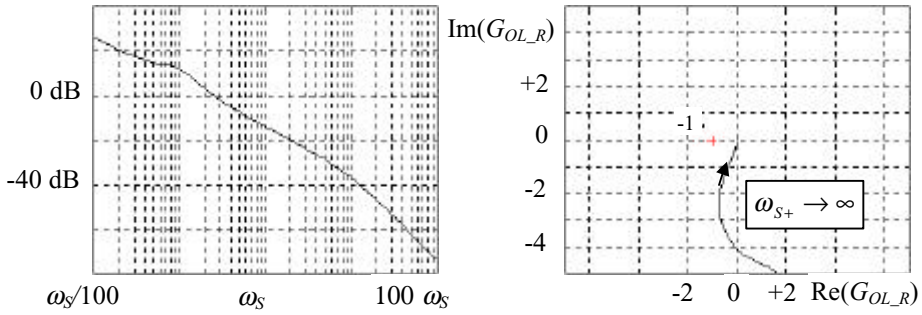

Figure 26: Open-loop Bode plot (left) and Nyquist diagram (right) for a radial loop with corrector associated to an AC-coupled beam phase loop (G_{PL0}=10ω_S, ω_{PH}= ω_{RL} = ω_S/10)

Close D-loop transfer function with corrector. Control of the radial position is properly achieved from DC to 0.3 ω_S (figure 27). Compared to the DC case (figure 21) or to the AC case without radial loop (figure 23), the operation of the beam phase loop is only slightly affected (figure 28) in the lower part of the frequency range, where the radial loop takes control.

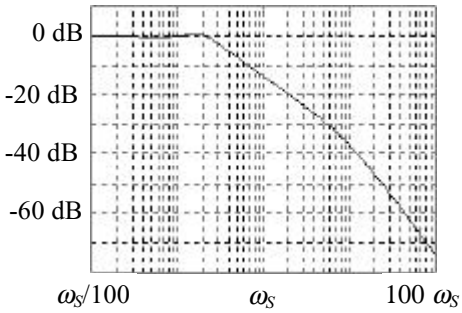

Figure 27: Closed-loop Bode plot for a radial loop with corrector associated with an AC-coupled beam phase loop: transmission of the $\Delta R/R_{prog}$ command onto $\Delta R/R$.

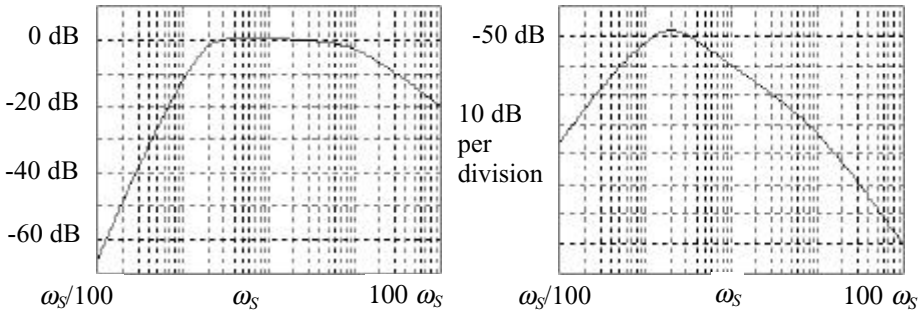

Figure 28: Closed-loop Bode plots for the AC-coupled beam phase loop in the presence of the radial loop: transmission of the $\Delta\varphi_{B\_prog}$ command onto $\Delta\varphi_B$ (left) and onto $\Delta R/R$ (right)

4.4 Synchronisation loop

The need frequently arises to synchronize the beam circulating in the synchrotron with an external RF reference, for instance for a "bunch-into-bucket" transfer into another machine.

Beam phase with respect to an external reference. The frequency of the external reference corresponds to a precise radial position. In Sec. 4.1 we have derived the relation between the beam radial position $\Delta R/R$ and $\Delta\varphi_B$. A relative frequency difference $\Delta\omega/\omega$ results from $\Delta R/R$, according to:

$$\frac{\Delta\omega}{\omega} = \left(\frac{\gamma_T^2 - \gamma^2}{\gamma^2}\right)\frac{\Delta R}{R} \tag{33}$$

Using Eqs. 29 and 30, we can deduce:

$$\Delta\omega = \left(\frac{\omega_S^2}{2\pi}\right)\frac{1}{s}\Delta\varphi_B \tag{34}$$

The frequency difference $\Delta\omega$ is the time-derivative of the phase φ_{SYN} of the beam with respect to the external reference. Consequently:

$$\Delta\omega = s \cdot \varphi_{SYN} \tag{35}$$

Combining Eqs. 34 and 35 we finally get the transfer function:

$$\frac{\varphi_{SYN}}{\Delta\varphi_B} = k_S \frac{1}{s^2} \tag{36}$$

with:

$$k_S = \frac{\omega_S^2}{2\pi} \tag{37}$$

The block diagram of a beam control equipped with a synchronisation loop is drawn in figure 29. Note that a beam phase loop is kept to provide damping of phase oscillations, while no radial loop can be maintained because the external frequency reference imposes a radial position.

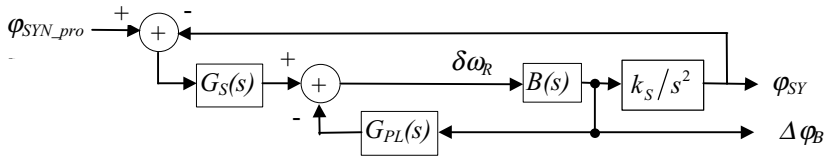

Figure 29: Block diagram of a synchronisation loop associated with a beam phase loop

Open-loop transfer function without corrector. The plots corresponding to a constant gain in $G_S(s)$ are presented in figure 30. The point (-1,0) is encircled by the gain curve in the Nyquist plot, so that the system is clearly unstable in closed loop. This is a direct consequence of the double integration from $\Delta\varphi_B$ to φ_{SYN}.

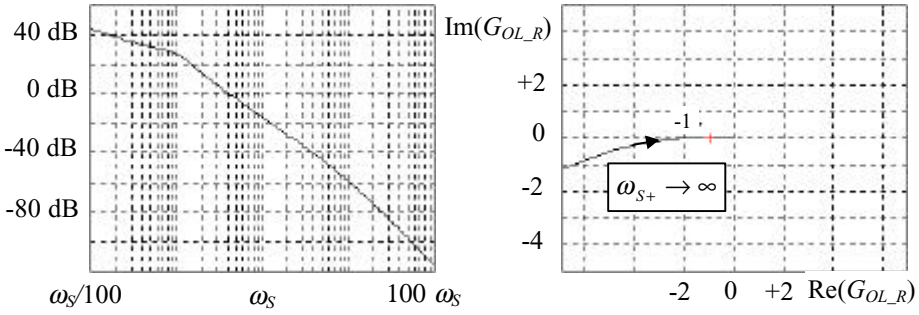

Figure 30: Open-loop Bode plot (left) and Nyquist diagram (right) for a synchronisation loop without corrector associated with an AC-coupled beam phase loop (G_{PL0}=10ω_S, ω_{PH}= ω_S/10, G_{S0}=10*ω_S)

Open-loop transfer functions with a corrector. Phase advance is obtained in the frequency range [ω_{SL}, ω_{SH}] where the open-loop gain crosses 0 dB ($\omega_{SL} < \omega_{SH}$) from a phase-lead network:

$$G_S(s) = G_{S0}\left(\frac{s+\omega_{SL}}{s+\omega_{SH}}\right) \tag{38}$$

The plots in figure 31 show that stability is now achieved.

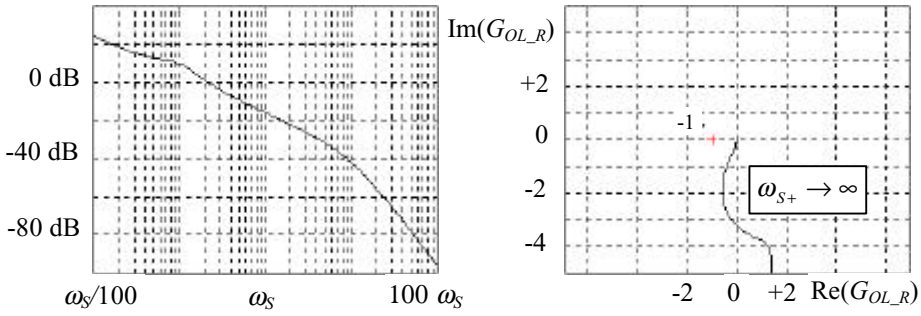

Figure 31: Open-loop Bode plot (left) and Nyquist diagram (right) for a synchronisation loop with corrector associated to an AC-coupled beam phase loop (G_{PL0}=10ω_S, ω_{PH}= ω_S/10, G_{S0}=100ω_S, ω_{SL}= ω_S/10, ω_{SH}=10ω_S)

Closed-loop transfer function. As shown in figure 32, the synchronisation loop gives control of φ_{SYN} to excitation from the φ_{SYN_prog} input. The response is low-pass, with a cut-off frequency at ~ 0.3 ω_S.

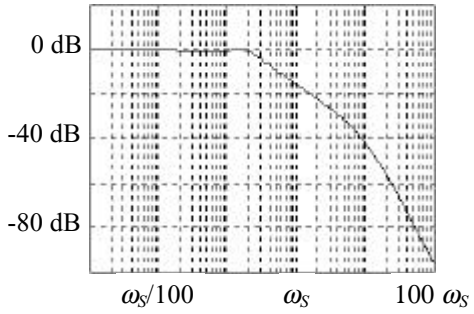

Figure 32: Closed-loop Bode plot for a synchronisation loop with corrector associated to an AC-coupled beam phase loop: transmission of the φ_{SYN_prog} command onto φ_{SYN}.

Operation of the beam phase loop is affected at low frequencies (figure 33 left to be compared to figures 21 and 23), but the response remains flat over the bandwidth. The effect of the phase loop command input $\Delta\varphi_{B\_prog}$ on the synchronisation phase

φ_{SYN} is negligible at very low frequencies (below ~ $\omega_S/100$), so that the static value of φ_{SYN} is fully under the control of the φ_{SYN_prog} input of the synchronisation loop. But for larger frequencies, especially slightly below and above the cut-off of the synchronisation loop, $\Delta\varphi_{B\_prog}$ is transmitted with a large gain to φ_{SYN}, so that care must be taken to limit noise on $\Delta\varphi_{B\_prog}$ in that frequency range.

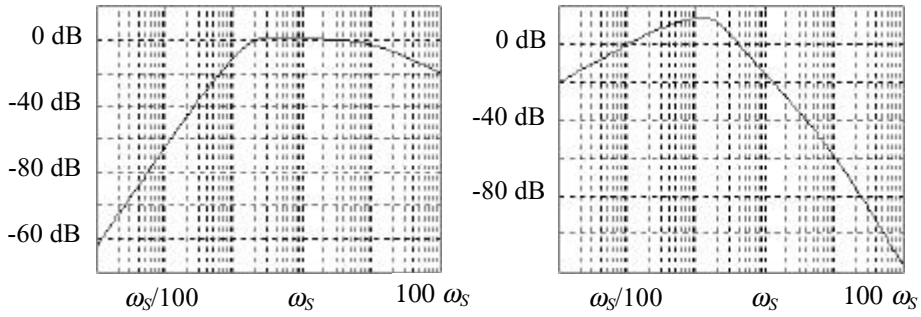

Figure 33: Closed-loop Bode plots for the AC-coupled beam phase loop in the presence of the synchronisation loop: transmission of the $\Delta\varphi_{B\_prog}$ command onto $\Delta\varphi_B$ (left) and onto φ_{SYN} (right)

5 High beam-intensity regime (Beam-loading effects and cures)

5.1 Conventions

Beam circulating in a synchrotron causes an image current I_B to flow on the vacuum chamber and through every obstacle along its path. RF cavities are especially important sources of impedance where this image current adds to the amplifier current I_G to develop voltage. Figure 34 shows the equivalent circuit and conventions used for the analysis [7].

$\vec{V}$: voltage across the cavity gap
$\vec{I}_G$: generator current (at the gap)
$\vec{I}_B$: beam current
$\vec{I}_T$: total current in the cavity
$\vec{I}_0$: resistive current

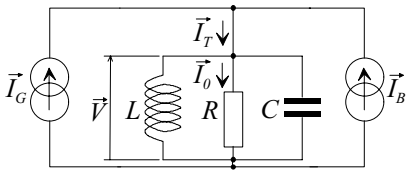

Figure 34: Equivalent circuit for a cavity

As a first approximation we will only consider the RF components of these beam currents. This is justified by the fact that the cavity impedance is, by construction, much larger at that frequency. Basic circuit equations and the vector diagram of the currents flowing in the cavity are represented in figure 35.

$$\vec{I}_T = \vec{I}_G + \vec{I}_B$$
$$\vec{I}_T = V \big/ Z_{cav} = V\left[1/R + j\left(C\omega - 1/(L\omega)\right)\right]$$
$$I_0 = V/R$$

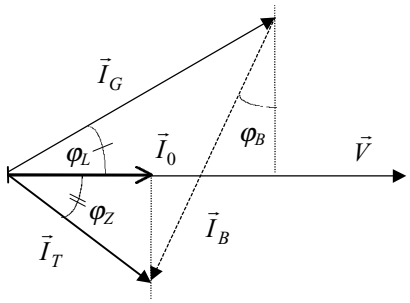

Figure 35: Basic equations and vector diagram (below transition) of the RF currents in a cavity

The amplitude of the beam RF current I_B depends upon the bunch spectrum, which itself results from the bunch length. In the limit of very short bunches, the RF component I_B is twice the DC beam current: $I_B = 2\ I_{B\_DC}$. The stable phase φ_B is defined as the phase providing the rate of energy-gain of the stable particle (Sec. 4.1). Beam loading is quantified using the dimensionless beam loading parameter Y defined by:

$$Y = I_B / I_0 \tag{39}$$

5.2 Beam loading effects

5.2.1 Tools for analysis

In the presence of beam loading, the voltage in a cavity is also influenced by the beam (figure 35). Consequently the cavity transfer functions for phase and amplitude modulations are modified, compared to the case studied in Sec.3.1, and new transfer functions relating the modulations induced on V by the phase modulation of I_B have to be considered. Derivation of these transfer functions is given in Appendix 2. The analysis of a typical RF system now involves the study of a flow-graph [7] as in figure 36, where there is a field amplitude (Sec.3.1.2) and a tuning (Sec. 3.1.3) control loop around the cavity, plus a beam phase loop (Sec. 4.2).

Phase and amplitude modulations are defined in Eq. 1, and they are labelled respectively (a_G, p_G) for the RF amplifier ("generator") and (a_V, p_V) for the cavity voltage. Only phase modulation p_B is considered for the beam. x is the tuning parameter defined in Eq. 9. The loop amplifiers and correction networks are included in C_a, C_t and C_p, respectively for the amplitude, tuning and beam phase loop.

The dashed lines in figure 36 correspond to coupling between loops. Couplings introduced by ${}^{G}G_{pa}$, ${}^{G}G_{ap}$ and G_{xa} have already been envisaged in Sec.3 in the case of a negligible beam current ($Y<<1$) and for one loop at a time.

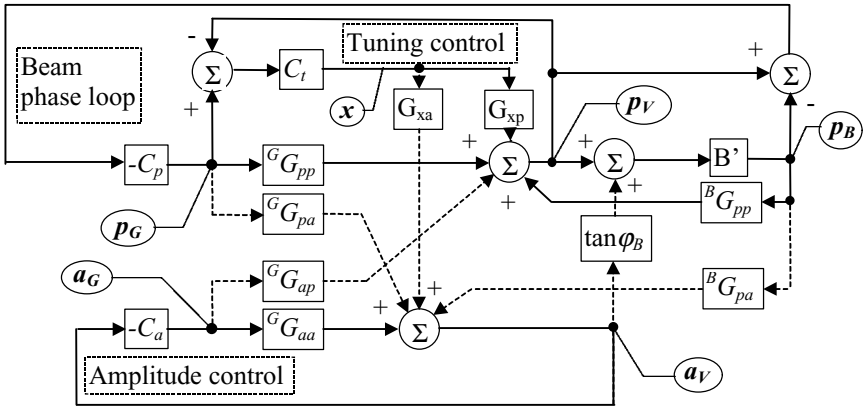

Figure 36: Flow graph of a complete RF system

The beam transfer function B derived in Sec. 4. (Eq. 26) corresponds to the transmission from $\delta\omega_{RF}$ (=-s.p_V) to (p_B-p_V). The beam transfer function B' used in figure 36 is slightly different because it relates p_B to p_V. Namely :

$$B = \frac{1 - B'}{s} \tag{40}$$

From Eqs. 26 and 40 we can obtain:

$$B' = \frac{\omega_S^2}{s^2 + \omega_S^2} \tag{41}$$

5.2.2 Robinson instability

Derivation. The simplest case is where there are no feedback loops (C_a=C_t=C_p=0). It corresponds to the canonical RF system represented in figure 1 (Sec. 2). The only remaining loops in the flow-graph of figure 36 are due to the effect of beam phase oscillations on the amplitude and phase of the cavity. Mason's rule applied to this system gives the following characteristic equation:

$$1 - B'.{}^{B}G_{pp} - B'.{}^{B}G_{pa}\tan\varphi_B = 0 \tag{42}$$

Replacing B', ${}^{B}G_{pp}$ and ${}^{B}G_{pa}$ by their expressions (Eq. 41 and Appendix 2) we finally get a fourth-degree polynomial equation:

$$s^4 + 2\sigma \cdot s^3 + \left[\omega_S^2 + \sigma^2\left(1 + \tan^2 \varphi_Z\right)\right] \cdot s^2 + 2\sigma\omega_S^2 \cdot s + \omega_S^2\sigma^2\left[1 + \tan^2 \varphi_Z - Y\frac{\tan\varphi_Z}{\cos\varphi_B}\right] = 0 \quad (43)$$

Looking for stability conditions, the Routh criteria gives the following inequalities in the case of an energy below transition ($\cos\varphi_B > 0$) :

$$0 < Y \sin 2\varphi_Z < 2\cos\varphi_B \quad (44)$$

These are called Robinson's instability limits [8]. Two different ranges of parameters are forbidden. The case $\varphi_B = 0$ deg is graphically illustrated in the co-ordinate system (φ_Z, Y) in figure 37.

Discussion. Instability in the left half of the plane is due to the cavity impedance, independently of the relative beam loading parameter Y. It corresponds to anti-damped in-phase dipolar oscillations of all bunches, and can also be derived from Sacherer's theory of instabilities [9].

The concave curve in the right half-plane is due to an RF power limitation and depends on Y. This corresponds to an aperiodic instability where the beam goes out of control without oscillation.

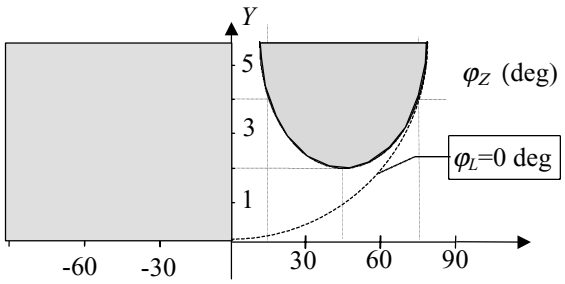

Figure 37: Robinson's instability diagram

Stability can always be attained for any value of Y, if the detuning of the resonator is made large enough. This is not as unreasonable as it may seem at first sight, once one notices that the curve corresponding to the best operating condition for the power amplifier (namely : φ_L = 0 deg) is always in the stable region and asymptotically approaches the concave limit when φ_Z tends towards 90 deg.

5.2.3 Multi-loop instability

The Robinson's instabilities represent a limit case, which is rarely encountered in real installations. The various loops described in Secs. 3 and 4 are generally present and must be taken into account. The full complexity of the flow graph in figure 36 has to be handled to derive the characteristic equation and analyse stability. Analytical solutions only exist for simplified limit cases.

Many examples have been treated in the literature, illustrating specific situations [4, 7]. A recurrent empirical observation that can be made is that the stability domain for systems containing a beam phase loop is often limited by a concave curve that extends over both side of the Y axis, with a minimum in the vicinity of $Y = 2$.

Similar cut-off frequencies must be avoided in the various loops, especially if they are near to the half-cavity bandwidth σ, because of the strong couplings it creates even at small values of Y.

Assuming that all loop amplifiers are simple integrators ($C_a = \omega_a$/s, etc...), and in the extreme case $\varphi_B = 0$ deg (stationary bucket), $\varphi_L = 0$ deg (amplifier driving a resistive load), σ large (wide band cavity), and B'(s) = 0 (rigid beam), F. Pedersen [7] has derived the following analytical criteria:

$$Y < \sqrt{2 + \frac{\omega_a}{\omega_T} + \frac{\omega_T}{\omega_a} + \frac{\omega_p}{\omega_T} + \frac{\omega_T}{\omega_p} + \frac{\omega_a}{\omega_p} + \frac{\omega_p}{\omega_a}} \tag{45}$$

5.3 Beam loading cures

5.3.1 Passive damping

The simplest method to reduce the relative beam loading $Y = I_B/I_0$ is to increase the resistive current I_0 in the cavity, but this solution is clearly inefficient due to the larger RF power required. However it is an easy means to obtain a moderate improvement factor in a small machine.

It has been implemented using a low output impedance RF amplifier, or even using a dummy load coupled to the cavity.

5.3.2 Feedforward

The principle of feedforward [10, 11, 12] is to use the RF amplifier itself to inject a current $-\vec{I}_B$ in the cavity. The equivalent impedance seen by the beam is then zero. This technique is illustrated in figure 38, where the input of the RF amplifier is driven by:

$$\vec{I}_G = \vec{I}'_G - \vec{I}_B \tag{46}$$

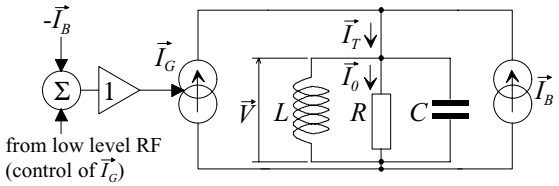

Figure 38: Layout of a feedforward beam-loading compensation

The low level RF system (beam control) controls $\vec{I}_T$ instead of $\vec{I}_G$ in the initial case. Cross-coupling between loops is largely reduced and system stability is largely improved. Some coupling remains due to the effect of $\vec{I}_B$ onto the tuning angle φ_L which the tuning loop regulates.

This method is inexpensive to implement, since it requires only slight modification to the low level RF hardware. But it is delicate to adjust and maintain, because it is an open-loop set-up and performance degrades with the drift of any element of the RF amplification chain.

5.3.3 Wideband feedback

The principle of wideband feedback [11-15] is to put the cavity inside a closed loop with a large loop gain (figure 39). That loop works directly at the RF and includes a high-gain and high-power amplification chain. The effect is a reduction of the apparent cavity impedance according to:

$$Z_{eq}(j\omega) = \frac{Z_{cav}(j\omega)}{1 + G_{OL}(j\omega)} \tag{47}$$

where $Z_{cav}(j\omega)$ is the cavity impedance (Eq. 4), $G_{OL}(j\omega)$ is the open loop gain and $Z_{eq}(j\omega)$ is the apparent impedance once the loop is closed. Assuming that the resonance frequency is the same in open and closed loop, the impedance at resonance is resistive and scaled by the factor 1/(1+A.g.R.Att). For a given beam intensity, the relative beam-loading parameter Y is then multiplied by the same factor. But efficiency stays similar to an open-loop system, contrarily to the case of passive damping (Sec. 5.3.1) where RF power is wasted.

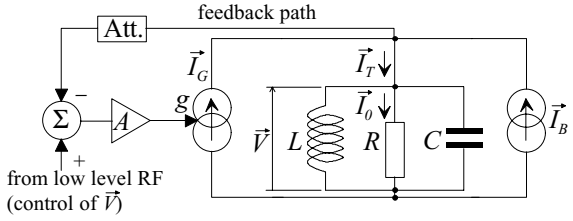

Figure 39: Layout of wideband feedback

System performance is limited by the electrical delay τ in the loop. It can be demonstrated [11, 12] that the minimum impedance at resonance is linked to the R/Q of the cavity and to τ by:

$$R_{eq\_\min} = \frac{2\omega_R}{\pi}\frac{R}{Q}\tau \tag{48}$$

With this technique the low level RF system has direct control of $\vec{V}$, which is the physical parameter really acting on the beam. It also has the advantage of being tolerant to drift in the characteristics of the elements by virtue of the feedback. A spurious effect is that the coupled-bunch instability thresholds are degraded because the real part of Z_{eq} is increased outside the loop bandwidth, and because the resonance frequency in closed loop can easily be offset from its open-loop value.

5.3.4 Long delay feedback

When reduction of the cavity impedance is required over a bandwidth of many revolution frequency harmonics, the wideband feedback scheme is limited by the electrical delay τ in the RF chain (effect leading to Eq. 48). But the beam spectrum is only made of narrow bands (a few synchrotron frequencies) around revolution harmonics, so that impedance reduction needs in fact to be effective over small bandwidths. A large delay can then be used in the RF chain, provided the loop has the proper phase for stability around every revolution harmonic. A delay of one machine turn clearly meets that criteria, and can be associated with a comb filter to make a "One-turn-delay feedback" system [11, 12, 16, 17] (figure 40).

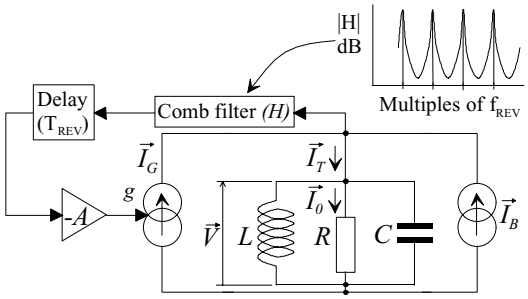

Figure 40 : Layout of ''One-turn-delay'' feedback

Implementation details. Care should be taken not to interfere with the operation of the other loops which all work in the vicinity of the RF frequency. This generally implies that the comb passband centred on the RF must be absent [16, 17].

An elegant solution for the comb filter is to use a digital recursive filter [16, 17] which has a transfer function given by :

$$H(j\omega) = \frac{G_0}{1 - Ke^{-j\omega T_{REV}}} \tag{49}$$

with K<1, using the one-turn delay $D(j\omega) = e^{-j\omega T_{REV}}$. The open loop gain is then :

$$G_{OL}(j\omega) = \frac{G_0 \cdot A \cdot g \cdot Z_{cav}(j\omega)}{e^{i\omega T_{REV}} - K} \tag{50}$$

More sophisticated operation is possible using digital signal processing. It has been applied to Linac RF systems, where the delay is the RF pulse repetition period, and is called ‘’Adaptive feedforward’’ [18, 19].

5.3.5 Comparison of cures

Table 2 summarises and compares the characteristics of the various cures described in the previous sections.

Table 2 : Comparison of cures against beam loading

Performance concerning :	**Passive damping**	**Feedforward***	**Fast feedback**	**Long delay feedback**
Beam loading at RF	Marginal improvement	Good	Excellent	Non relevant
Transient beam loading	Small effect	Can be good (difficult to adjust)	Small effect	Excellent
Spurious effects for the beam	None	Can be favorable against instabilities (difficult to adjust)	Degrades instabilities threshold	Improves instabilities threshold
Complexity	Small	Small / Medium	High	Medium
Adjustment	Easy	Lengthy (with beam)	Easy (on bench)	Easy (on bench)
Drift of characteristics	No	Yes	No	No
Range (in β and h)	Unlimited	Limited for good performance	Unlimited	Unlimited
Cost	High	Small	Medium	Small
Ease of operation	Easy	Complex	Easy	Easy

* Remark : comments on the feedforward method assume that the beam signal is fed at the low power end of the amplification chain which implies a long delay. Better ratings apply when the electrical delay is small [20].

Appendix 1 : Transfer functions for tuning

Cavity impedance

The cavity being approximated by an RLC parallel circuit, its impedance Z is given by Eq. 4:

$$Z(s) = \frac{2\sigma Rs}{s^2 + 2\sigma s + \omega_R^2}$$

where ω_R (rad/s) is the resonant frequency, Q is the quality factor ($Q = R\sqrt{C/L}$), and σ is the damping rate ($\sigma = \omega_R/(2Q)$ is also the half 3 dB bandwidth).

For ω_C in the vicinity of ω_R :

$$Z(j\omega_C) = \frac{2j\sigma R\omega_C}{\omega_R^2 - \omega_C^2 + 2j\sigma\omega_C} \approx \frac{R}{1 - j\tan\varphi_Z} \tag{51}$$

using the definition : $\tan\varphi_Z = \dfrac{\omega_R - \omega_C}{\sigma}$ (52)

Effects of a variation dx of the tuning parameter

The normalised tuning parameter x is defined by Eq. 9, and using Eq. 52 we get: $x = \tan\varphi_Z$ so that : $dx = d(\tan\varphi_Z)$.

At constant excitation current and for a change dx, the amplitude V and phase φ of the cavity voltage are modulated by :

$$\begin{aligned} \frac{dV}{V} &= \frac{d|Z|}{|Z|} = \frac{1}{|Z|}\frac{d|Z|}{dx}dx \\ d\varphi &= \frac{dArg(Z)}{dx}dx \end{aligned} \tag{53}$$

Using the expression given for Z as a function $\tan\varphi_Z$, the derivatives with respect to x are :

$$\frac{1}{|Z|}\frac{d|Z|}{dx} = \frac{-\tan\varphi_Z}{\left(1 + \tan^2\varphi_Z\right)} \tag{54}$$

$$\frac{d(Arg(Z))}{dx} = \frac{d\varphi_Z}{dx} = \frac{1}{(1 + \tan^2\varphi_Z)} \tag{55}$$

Transmission of the effects of dx

The amplitude and phase modulations generated by dx are fed into the resonator. They are transmitted with the transfer functions G_S and G_C characterising the cavity (Eq. 5 in Sec. 3.1.1). Consequently :

$$\begin{aligned} G_{xa} &= \frac{a}{dx} = \frac{1}{|Z|}\frac{d|Z|}{dx}G_S + \frac{dArg(Z)}{dx}G_C \\ G_{xp} &= \frac{p}{dx} = \frac{dArg(Z)}{dx}G_S - \frac{1}{|Z|}\frac{d|Z|}{dx}G_C \end{aligned} \tag{56}$$

Substituting into these formulas the expressions obtained earlier for the derivatives with respect to x, we finally obtain :

$$G_{xa} = \frac{-\sigma^2 \tan\varphi_Z}{s^2 + 2\sigma s + \sigma^2(1+\tan^2\varphi_Z)}$$
$$G_{xp} = \frac{\sigma^2 + \sigma s}{s^2 + 2\sigma s + \sigma^2(1+\tan^2\varphi_Z)} \quad (57)$$

Appendix 2 : Transfer functions in the presence of beam loading

The transmission of the modulations of I_G onto V is deduced in two steps. In the first step, the transmission onto the total current I_T is derived. In the second, the modulations of V resulting from the ones of I_T are obtained.

Transmission of modulations of I_G onto I_T

From Eq. 2 we can write :

$$I_G(t) = \mathrm{Re}\left\{I_G e^{j\omega_C t}\left[1 + a_G(t) + j \cdot p_G(t)\right]\right\} \quad (58)$$

It is equivalent to saying that the vector $\vec{I}_G$ is modulated in amplitude by a parallel vector of length $\Delta I_{G//} = a_G I_G$. Similarly, the vector $\vec{I}_G$ is modulated in phase by a perpendicular vector of length $\Delta I_{G\perp} = p_G I_G$. This is illustrated in the vector diagram in figure 43.

The modulations of I_T can be deduced geometrically from the ones of I_G:

$$\Delta I_{T//} = \Delta I_{G//}\cos\varphi_{GT} - \Delta I_{G\perp}\sin\varphi_{GT}$$
$$\Delta I_{T\perp} = \Delta I_{G//}\sin\varphi_{GT} + \Delta I_{G\perp}\cos\varphi_{GT} \quad (59)$$

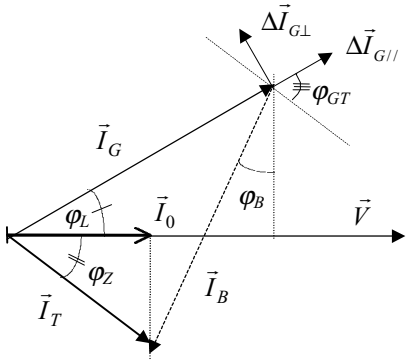

Figure 43: Vector diagram for the transmission of modulations of I_G

Consequently:

$$\begin{aligned} a_T &= \frac{\Delta I_{T//}}{I_T} = \frac{I_G}{I_T}\left(a_G \cos\varphi_{GT} - p_G \sin\varphi_{GT}\right) \\ p_T &= \frac{\Delta I_{T\perp}}{I_T} = \frac{I_G}{I_T}\left(a_G \sin\varphi_{GT} + p_G \cos\varphi_{GT}\right) \end{aligned} \tag{60}$$

Transmission of modulations of I_T onto V

By definition of the modulation transfer functions (Sec. 3):

$$\begin{aligned} a_V &= a_T G_{aa} + p_T G_{ap} \\ p_V &= p_T G_{pp} + a_T G_{pa} \end{aligned} \tag{61}$$

Using the previous expressions for a_T and p_T as a function of a_G and p_G we can write:

$$\begin{aligned} a_V &= a_G \frac{I_G}{I_T}\left[G_{aa}\cos\varphi_{GT} + G_{ap}\sin\varphi_{GT}\right] + p_G \frac{I_G}{I_T}\left[G_{ap}\cos\varphi_{GT} - G_{aa}\sin\varphi_{GT}\right] \\ p_V &= p_G \frac{I_G}{I_T}\left[G_{pp}\cos\varphi_{GT} - G_{pa}\sin\varphi_{GT}\right] + a_G \frac{I_G}{I_T}\left[G_{pp}\sin\varphi_{GT} + G_{pa}\cos\varphi_{GT}\right] \end{aligned} \tag{62}$$

The transfer functions for *IG* to *V* in the presence of beam loading are then:

$$\begin{aligned} {}^{G}G_{aa} &= {}^{G}G_{pp} = \frac{I_G}{I_T}\left[G_{aa}\cos\varphi_{GT} + G_{ap}\sin\varphi_{GT}\right] \\ {}^{G}G_{pa} &= -{}^{G}G_{ap} = \frac{I_G}{I_T}\left[G_{pa}\cos\varphi_{GT} + G_{aa}\sin\varphi_{GT}\right] \end{aligned} \tag{63}$$

Replacing these transfer functions with their expression for a cavity (Eq. 5) and using geometric considerations we finally get:

$$\begin{aligned} {}^{G}G_{aa} &= {}^{G}G_{pp} = \frac{\sigma^2\left[1+\tan^2\varphi_Z + Y\left(\sin\varphi_B - \tan\varphi_Z\cos\varphi_B\right)\right] + \sigma\left(1 + Y\sin\varphi_B\right)s}{s^2 + 2\sigma s + \sigma^2(1+\tan^2\varphi_Z)} \\ {}^{G}G_{pa} &= -{}^{G}G_{ap} = \frac{-\sigma^2 Y\left(\cos\varphi_B + \tan\varphi_Z\sin\varphi_B\right) + \sigma\left(\tan\varphi_Z - Y\cos\varphi_B\right)s}{s^2 + 2\sigma s + \sigma^2(1+\tan^2\varphi_Z)} \end{aligned} \tag{64}$$

Transmission of modulations of I_B onto V

In a similar way, the following relations can be established for the transmission of the modulations of I_B onto V:

$$
\begin{aligned}
{}^{B}G_{aa} = {}^{B}G_{pp} &= \frac{Y\left[\sigma^2(\tan\varphi_Z\cos\varphi_B - \sin\varphi_B) - \sigma\sin\varphi_B s\right]}{s^2 + 2\sigma s + \sigma^2(1+\tan^2\varphi_Z)} \\
{}^{B}G_{pa} = -{}^{B}G_{ap} &= \frac{Y\left[\sigma^2\left(\cos\varphi_B + \tan\varphi_Z\sin\varphi_B\right) + \sigma\cos\varphi_B s\right]}{s^2 + 2\sigma s + \sigma^2(1+\tan^2\varphi_Z)}
\end{aligned}
\qquad (65)
$$

References

1. J.J. D'Azzo, Constantin H. Houpis, 'Linear Control System Analysis and Design', McGraw-Hill, 1981.
2. P.F. Panter, 'Modulation, Noise and Spectral Analysis', McGraw-Hill, 1966.
3. R. Garoby, Proc. of the CERN Accelerator School 'RF Engineering for Particle Accelerators', Oxford, Apr. 1991, CERN 92–03 (1992).
4. D. Boussard, Proc. of the CERN Accelerator School 'RF Engineering for Particle Accelerators', Oxford, Apr. 1991, CERN 92–03 (1992).
5. J.M. Brennan, 'RF Beam Control for the AGS Booster', BNL-52438, Sept. 1994.
6. F. Blas et al., 'Digital Beam Controls for Synchrotrons and Storage Rings in the CERN PS Complex', Proc. of EPAC94 - London (GB), pp. 1568-1570.
7. F. Pedersen, 'Beam Loading Effects in the CERN PS Booster', IEEE Trans. Nuc. Sci., NS-22, 1975, p. 1906.
8. K.W. Robinson, 'Stability of beam in Radiofrequency System', CEAL-1010, Feb. 1964.
9. F.J. Sacherer, 'A Longitudinal Stability Criterion for Bunched Beams', IEEE Trans. Nuc. Sci., NS-20, 1973, p. 825.
10. D. Boussard, 'Cavity Compensation and Beam Loading Instability', CERN/SPS/ARF Note 78-16.
11. D. Boussard, 'Control of Cavities with High Beam Loading', Proc. of PAC85 - Vancouver (Canada), IEEE NS-32, No. 5, Oct. 85, pp. 1852-1856.
12. R. Garoby, 'Beam Loading in RF Cavities', Lecture Notes in Physics 400, Frontier of Particle Beams: Intensity Limitations, Springer Verlag 1992, pp.509-541.
13. F. Pedersen, 'RF Cavity Feedback', Proc. of Conf. On B Factories - Stanford (USA), 1992, CERN/PS 92-59 (RF).
14. F. Ferger, W. Schnell, 'The High Power Part of the RF System for the ISR', 2nd Natl. Conf. On Part. Acc., Moscow, Sept. 1970.
15. R. Garoby et al., 'RF System for High Beam Intensity Acceleration in the CERN PS', Proc. of PAC89 - Chicago (USA), pp. 135-137.

16. D. Boussard, G. Lambert, 'Reduction of the Apparent Impedance of Wide-Band Accelerating Cavities by RF Feedback', IEEE Trans. Nuc. Sci., NS-30, 1983, p. 2239.
17. F. Blas, R. Garoby, 'Design and Operational Results of a "One-Turn-Delay" Feedback for Beam Loading Compensation of the CERN PS ferrite Cavities', Proc. of PAC91 - San Francisco (USA), pp. 1398-1400.
18. S.P. Jachim, E.F. Natter, 'Beam Loading and Cavity Compensation for the Ground Test Accelerator', Proc. of PAC89 - Chicago (USA), pp. 1870-1873.
19. C.D. Ziomek, 'Adaptive Feedforward in the LANL RF Control System', Proc. of LINAC92 - Ottawa (Canada), pp. 683-685.
20. S. Ninomiya et al., 'The RF Power System with Beam Loading Cancellation for the KEK-PS Booster', Proc. of the 14th Intl. Conf. On High Energy Accelerators, Particle Accelerators, 1990, Vol. 32, p. 69.